Chapter 8

Overview of Solar-Forecasting Methods and a Metric for Accuracy Evaluation

Carlos F.M. Coimbra and Jan Kleissl
Center for Renewable Resources and Integration, Department of Mechanical and Aerospace Engineering, University of California, San Diego

Ricardo Marquez
SolAspect

Chapter Outline

8.1. Classification of Solar-Forecasting Methods 172
8.2. Deterministic and Stochastic Forecasting Approaches 177
8.2.1. A Critical Appraisal of Physically-Based Forecasting Approaches 177
8.2.2. Satellite Forecasts 178
8.2.3. Sky-Imager Forecasts 179
8.2.4. Data Inputs to Stochastic-Learning Approaches 179
8.2.5. Section Summary 181
8.3. Metrics for Evaluation of Solar-Forecasting Models 182
8.3.1. Solar Resource Variability 182
8.3.2. Conventional Metrics for Model Evaluation 183
8.3.3. A Time Horizon–Invariant (THI) Metric 185
8.4. Applying the THI Metric to Evaluate Persistence, and Nonlinear Autoregressive Forecast Models 187
8.4.1. NAR and NARX Forecasting Models 187
8.4.2. Comparison of Forecasting Models and Persistence 188
8.4.3. Comparison with a Satellite Cloud-Motion Forecast Model 191
8.5. Conclusions 191
References 192

Solar Energy Forecasting and Resource Assessment. ISBN: 9780123971777

8.1. CLASSIFICATION OF SOLAR-FORECASTING METHODS

Load forecasts have been an integral part of managing electrical-energy markets and infrastructure for many decades. Consequently, experiences, regulations, and planning by utilities and independent system operators (ISO) are the dominant considerations for research and commercial development in this field. Because the rules established by ISOs will impact the economic value of forecasting to other stakeholders such as owner-operators, in the near term the primary stakeholders for forecasting needs and plans are ISOs. Secondary stakeholders are utilities that are seeing greater distributed PV penetration on their urban distribution feeders. Currently only a few utilities have mechanisms for using solar forecasts for local automated response to voltage fluctuations caused by variable solar production.

The choice of solar-forecasting method depends strongly on the timescales involved, which can vary from horizons of a few seconds or minutes (intrahour), a few hours (intraday), or a few days ahead (intraweek). Different time horizons are relevant according to the forecast application. As an example, the California Independent System Operators (CAISO) organization uses the following forecasts. The day-ahead (DA) forecast is submitted at 0530 prior to the operating day, which begins at midnight on the day of submission and covers (on an hourly basis) each of the 24 h of that operating day. Therefore, the DA forecast is provided 18.5 to 42.5 h prior to the forecasted operating day. The vast majority of conventional generation is scheduled in the DA market. The hour-ahead (HA) forecast is submitted 105 min prior to each operating hour. It also provides an advisory forecast for the 7 h after the operating hour. CAISO is considering the implementation of intrahour forecasts at 5 min intervals; a similar intrahour forecast is already implemented by the Midwest ISO. The Federal Energy Regulatory Commission (FERC) has issued a Notice of Proposed Rulemaking requiring public utility transmission providers to offer all customers the opportunity to schedule transmission service every 15 min, and requiring providers with variable renewables in their systems to use power-production forecasting. In summary, intraday forecasts are currently of smaller economic value than are DA forecasts; however, with increasing solar penetration and the expected accuracy improvement of intraday compared to DA forecasts, substantial market opportunities will likely materialize.

For this reason, medium-term (<48 hours) solar forecasts are useful for energy resource planning and scheduling whereas intraday forecasts are useful for load following and predispatch, reducing the need for frequency control ("regulation") in "real" time.

The type of solar resource to be forecast depends on the technology (Table 8.1). For *concentrating solar systems* (concentrating solar-thermal or concentrating PV, CPV), the direct normal incident irradiance (DNI) must be forecast. Because of nonlinear dependence of concentrating solar-thermal efficiency on DNI and the controllability of power generation through

TABLE 8.1 Important Variables in Solar Forecasting

Forecast variable	Application	Primary determinants	Importance to market	Current forecast skill
GI	PV	Clouds, solar geometry	High	Medium
Cell temperature	PV	GI, air temperature, wind	Low	High
DNI	Concentrating solar power	Clouds, aerosols, water vapor	Medium	Low

thermal energy storage (if available), DNI forecasts are especially important for the management and operation of concentrating solar thermal power plants. DNI is impacted by phenomena that are very difficult to forecast, such as cirrus clouds, wildfires, dust storms, and episodic air pollution events, which can reduce DNI by up to 30% on otherwise cloud-free days.

For *nonconcentrating systems* (i.e., most PV systems), primarily global irradiance (GI = diffuse + direct) on a tilted surface is required, which is less sensitive to errors in DNI since a reduction in clear-sky DNI usually results in an increase in diffuse irradiance. For higher accuracy, forecasts of PV-panel temperature are needed to account for the (weak) dependence of solar-conversion efficiency on PV-panel temperature (see Table 8.1).

For relatively longer time horizons of the order of 6 h or more, physics-based models are typically employed (Table 8.2; Hammer et al., 1999, 2001, 2003; Perez et al., 2010; Lorenz et al., 2009). In the 2–6 h time horizons, a combination of methods is used that relies on observations or predictions of clouds through numerical weather predication (NWP) models (Figure 8.1; Lorenz et al., 2009), especially those in "rapid-refresh" mode, and satellite images with cloud optical depth and cloud-motion vector information (Hammer et al., 1999, 2001, 2003). For the very short term (<30 min), a number of techniques based on ground-to-sky imagers have been developed for both GHI and DNI (Chow et al., 2011, Marquez & Coimbra 2012, Marquez et al., 2013) by converting the cloud-positioning information into deterministic models. At shorter time horizons (<2 h), forecasting applications tend to rely more on statistical approaches, such as autoregressive integrated moving averages (ARIMA) and artificial neural network (ANN) modeling (Sfetsos & Coonick, 2000, Cao & Lin. 2008, Crispim et al., 2008, Reikard 2009, Paoli 2010, Mellit et al., 2010, Marquez & Coimbra 2011, Pedro & Coimbra 2012). Since the "hand-over" time between different methods is not constant, dynamic (regime-based) blends of different approaches ultimately offer the greatest accuracy

TABLE 8.2 Characteristics of and Inputs for Solar-forecasting Techniques

Technique	Sampling rate	Spatial resolution	Spatial extent	Suitable forecast horizon	Application
Persistence	High	1 point	1 point	Minutes	Baseline
Total-sky imagery	30 s	10 s–100 m	2–5 m radius	Tens of minutes	Short-term ramps, regulation
GOES satellite imagery	15 min	1 km	U.S.	5 hours	Load following
NAM weather model	1 h	12 km	U.S.	10 d	Unit commitment

(Chen et al., 2011; Marquez & Coimbra 2011). For example, at shorter forecast horizons, ANN time series–based forecasts are competitive in terms of overall error with satellite-based models (Marquez et al., 2012). Ultimately, statistical postprocessing that includes stochastic-learning techniques to dynamically assemble or correct different input forecasts typically improves forecast accuracy. For example, to improve site-specific forecast accuracy, forecasts

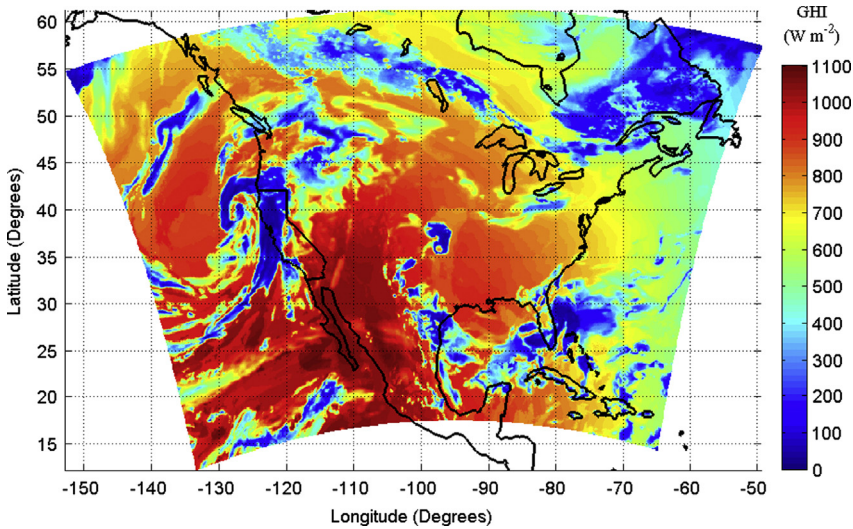

FIGURE 8.1 Forecast GHI (W m^{-2}) on April 10, 2010, at midday from the North American Mesoscale model (NAM). *This figure is reproduced in color in the color section.*

derived from NWP models can be corrected using model output statistics (MOS) (Mathiesen & Kleissl 2011, Lorenz et al., 2009).

The chapters dealing with solar forecasting in this book provide a comprehensive overview of forecasting techniques. For short-term forecasting, sky-imaging methods (Chapter 9) and stochastic-learning methods (Chapter 15) are presented. While solar radiometers or power output at a site contain no *direct* information about future output (e.g., a large cloud may be about to pass over the power plant, but the measurement is still clear), sky imagery allows visualizing the cloud field and cloud speed with respect to the solar plant. Clouds can be assigned motion vectors and optical depth to obtain forecasts up to 30 min ahead. Stochastic-learning methods in their simplest implementation require no ancillary (exogenous) data, but can learn patterns in power output that can be applied to derive likely future behavior. For example, the persistent burnoff of marine-layer clouds in coastal California in the late summer morning can be learned by stochastic models. More advanced models can also be trained to learn more complex features.

Modern satellite solar-forecasting tools rely on semi-empirical (Chapter 2) and physically based (Chapter 3) approaches to estimate the solar resource, and combine these approaches with cloud-motion vectors (Chapters 10, 11). Persistence in cloud optical depth and speed are assumed to yield future cloud locations and solar forecasts. Semi-empirical methods treat the atmosphere as one layer; the reflectance is measured for each pixel, and the resulting cloud index is related to ground-based GHI based on empirical calibrations. Physically based approaches simulate radiative transfer through different layers in the atmosphere and take advantage of the abilities of modern satellite remote sensing to determine, for example, cloud heights and types, aerosol optical depth, and water vapor. However, errors in satellite observations and the complexity of radiative transfer can cause physically based methods to underperform.

Numerical weather prediction is the ultimate physically based forecasting tool (Chapters 12, 13, 14). All physical processes (pressure, wind, temperature, water-vapor condensation and evaporation, and radiative transfer of solar and longwave radiation), along with their feedback, are described through physical models. NWP simulation codes consist of tens of thousands of lines of code that have evolved through decades of research. Supplied with the right initial conditions (three-dimensional atmospheric properties) and run fine enough to resolve the physical processes (micrometers), NWP models are able to simulate the atmosphere exactly. However, great shortcomings exist in available measurements of the initial state (motivating data assimilation in Chapter 13) and in the computational resources to run at a high enough resolution. Consequently, NWP forecasts are inferior for short time horizons. They are provided operationally by government centers such as NOAA, ECMWF, and GEMS, where each center typically uses a different model with

different parameterizations and measurement inputs. These model runs are generally not optimized for a specific location or for solar forecasting, but rather for predicting extreme weather events, temperatures, and aviation weather. Consequently, accuracy can be improved by locally running dedicated NWP models such as the Weather Research and Forecasting (WRF) model. Such runs offer the user the opportunity to choose the appropriate model resolutions, parameterizations, and postprocessing tools to optimize forecast accuracy (Chapter 14).

Time series-based methods, including regression methods such as ARIMA and nonlinear model approximators such as ANNs, are categorized as stochastic. When developing these approaches, it is postulated that a function exists that can be used to forecast future values based on previous values of the time series under consideration and/or other time-series variables. The stochastic class of solar-forecasting methods includes data-driven approaches that are developed by fitting the parameters of the model function in a training phase with input and target data. Examples can be found in Cao & Lin 2008, Crispim et al., 2008, Mellit 2008, Bacher et al., 2009, Reikard 2009, Paoli 2010, Sfetsos & Coonick 2000, Mellit & Pavan 2010, Chen et al., 2011, Marquez & Coimbra 2011, Pedro & Coimbra 2012). The rationale for these data-driven approaches is that patterns exist in the historical dataset that can be exploited for forecasting. Furthermore, these approaches allow the model developer to easily include more predictor variables as needed to improve forecast capability.

A recommendation for the best solar-forecasting approach is well summarized by Schroedter-Homscheidt et al., (2009), who propose to use

- Deterministic NWP schemes in the day-ahead market with ensemble prediction technologies for GHI and DNI.
- Aerosol optical depth modeling from air-quality applications in day-ahead prediction (primarily for DNI).
- Nowcasting of cloud fields and irradiance from satellites. Cloud-motion vector forecasting, including both visible and infrared channels, should be used for the 1–5 h forecast horizon (satellite-based aerosol added for DNI).
- Ground measurements for intrahour forecasts.

Ideally, each forecasting model derived from the different inputs is optimized through stochastic-learning techniques that remove bias and learnable errors from the deterministic models as data collection and forecasting assessments progress.

Forecasting inacuracies have different economic consequences depending on the time horizon and application. It is therefore important to develop forecasting metrics that are applicable to each (or all) forecasting time horizon involved and that reflect appropriate measures of forecasting skill according to readily computable quantities. Moreover, to intercompare forecasting approaches that are typically applied to different locations or at least to

different time periods, the ideal forecasting-skill metrics should be independent of the specific meteorological or climatological characteristics of the site under consideration. In Section 8.4 we exploit a simple set of metrics that can be used to compare the effectiveness of different forecasts.

8.2. DETERMINISTIC AND STOCHASTIC FORECASTING APPROACHES

8.2.1. A Critical Appraisal of Physically-Based Forecasting Approaches

Both physically based and deterministic (PB) solar-forecast and stochastic approaches are important for achieving the best overall forecast; their integration is generally the holy grail. Physically based forecasts are often more appealing to the scientifically curious mind as they express and allow the analysis of fluid, thermodynamic, and heat-transfer processes. For example, a three-dimensional radiative-transfer model can very accurately simulate diffuse- and direct-irradiance distributions and can be tested against measurements or first principles. PB approaches leave the human "in the driver"s seat"; humans can provide their input directly into the forecast, such as defining model components and detecting and tracking forecast errors based on recognizable input/output relationships. PB models are also more amenable to sharing (as for example in the WRF community model), as in principle the performance and application of the model should not depend on local conditions or appropriate training.

However, PB forecasts have several shortcomings primarily related to insufficient data to force the models and insufficient computational resources to accurately model all processes from first principles. Our application of solar forecasting would require measurements (for initial conditions) and modeling of the entire Earth's atmosphere at resolutions of aerosol particles or cloud droplets, which are in the order of micrometers. This is impossible because ground-measurement networks are much too sparse and mostly sample only the atmospheric surface layer or integrated atmospheric properties (such as aerosol optical depth) that do not allow vertical allocation of, say, a dust cloud. Even geostationary satellites have only spatial resolutions O(km). Consequently, NWP models do not have sufficient information for initial conditions. This is in itself a critical limitation that results from the chaotic nature of atmospheric processes. In addition, the coarse NWP resolution of O (10 km) causes crude representations of clouds through parameterizations. Grid cells are typically assumed to be either filled or not filled by blocky clouds at least 1-model-layer thick. All cloud properties are lumped into an optical depth and an albedo for each layer that are both parameterized using a separate cloud model. Optical depth and albedo depend only on water-mixing ratios (primarily liquid and ice), temperature, and pressure. Ozone and other trace-gas concentrations from

climatological tables are typically used. For computational efficiency, radiative transmission is subsequently calculated only on an hourly time step in an assumed plane-parallel atmosphere with homogeneous layers. In other words, the model is strictly one-dimensional—GHI is affected only by conditions present in the column of atmosphere directly above the grid point. As is evident, the physical variables are not represented with adequate accuracy. In addition, PB models are relatively static since the complexity of the underlying physics and the models written to describe them causes strong interactions between model components that make changes cumbersome. As a result, PB models do not directly or automatically learn from previous deviations and are sensitive to bias and systematic errors.

8.2.2. Satellite Forecasts

Satellite forecasts are typically a hybrid implementation of PB and stochastic approaches. Since the measurements provide (reflected) solar radiances directly, compared to NWP only a few relatively simple modeling assumptions have to be applied to derive the solar resource (see Chapter 2 also on the intricacies of deriving accurate *long-term* resource maps from satellite data). Satellite cloud-motion vector models are in fact mostly stochastic in that persistence of cloud speed and direction (as derived from the two last images) is assumed. The dynamic nature of clouds challenges cloud-motion vector approaches as cloud distribution can change substantially within the 30 min horizon that is the typical rate of image refresh. It is therefore challenging to account for cloud convection, formation, dissipation, and deformation. However, since large-scale cloud *systems* (such as those associated with a cold front) are more persistent, satellite-based forecasts typically perform more accurately than NWP-based forecasting models up to 6 h ahead, mostly because of ingestion, data assimilation, and latency of calculations required to "spin up" NWP-based forecasts.

Improvements in satellite forecasting can leverage synergy between NWP and satellite forecasts. For longer lookahead times, wind fields from NWP can be used to improve on the steady cloud advection vectors from two recent images (Miller et al., 2011), but the benefit of the approach has yet to be widely demonstrated. Conversely, satellite-derived motion vectors are being used to improve NWP forecasts. For example, Velden et al (1998) showed that GOES multispectral wind information has a significant positive impact on numerical model–derived forecasts for tropical cyclone tracks.

Classical satellite methods use only the visible channels (i.e., they work only in daytime), which makes morning forecasts less accurate because of a lack of time history. To obtain accurate morning forecasts, it is important to integrate infrared channels (which work day and night) into the satellite cloud motion forecasts (Chapters 10 and 11).

8.2.3. Sky-Imager Forecasts

Sky imagery (SI) has the advantage of providing very detailed information about the extent, structure, and motion of existing clouds at the time the forecast is made. These data can be used to generate very short term (minutes ahead) predictions of future cloud patterns in the vicinity of the solar-generation facility. However, like satellite forecasts, SI-forecasting methods at present do not account for cloud development and dissipation or significant changes in cloud geometry. The extrapolation of cloud patterns is also limited to the spatial scale defined by the SI field of view, but forecasts from clouds at shallow view angles suffer from bad perspective. The actual lookahead time for which SI has significant skill mostly depends on cloud height and velocity, since the ratio of cloud velocity to cloud height approximates an angular velocity about the SI that determines the time the cloud is in the field of view. The sight length divided by typical cloud speeds places the maximum time horizon for SI-based forecasts around 30 min, with maximum forecasting skills occurring in the 5–10 min range. Even if cloud size and velocity could be determined accurately, forecast accuracy depends on the rate at which the cloud field is departing from the static advection defined by the cloud-motion vectors (development, dissipation, etc.).

For intrahour forecasts, SI is constrained at the lower limit (typically 0–3 min) by sensor saturation near the Sun (which affects cloud definition) and image-processing latency times. At the upper limit, deterministic models based on sky imaging are limited by the extent of the field of view, and cloud speed and lifetimes. At UC San Diego, SIs have recently been specifically developed for solar-forecasting applications and feature high-resolution, high dynamic range, and high-stability imaging chips that enable cloud-shadow mapping and solar forecasting at unprecedented spatial detail (Chapter 9). Such cameras are better able to resolve clouds near the Sun and near the horizon, which extends forecast accuracy, especially for very short and very long lookahead times.

8.2.4. Data Inputs to Stochastic-Learning Approaches

In general, stochastic approaches can more easily incorporate information about phenomena at various timescales; thus, a time-horizon limitation mostly depends on the available historical data for the training stages, but also depends on the temporal autocorrelation function of the input variables. As discussed in Chapter 15, stochastic methods for solar irradiance may make use of any one or several of the following as input variables: clear-sky irradiance models, solar-geotemporal variables, NWP-derived cloud cover and other meteorological fields, satellite data, sky imagers, historical solar-irradiance values, and other ground-measured meteorological data. Because stochastic methods do not necessarily rely on a closed-form model, the ability to select relevant inputs for inclusion in the model is critical. Although clouds typically have the strongest

effect on solar irradiance at ground level, other meteorological inputs such as aerosols (Breitkreuz et al., 2009), and sky infrared measurements obtained from ground infrared sensors (Marquez et al., 2013) can provide useful information for the forecasting model. More notably, lagged/time-delay values of measured solar-irradiance time series are almost always included as inputs into stochastic modeling approaches (Mellit 2008). Other meteorological inputs such as temperature, relative humidity, and probability of precipitation obtained from NWP models have been shown to provide useful information for improved solar-irradiance forecasting (Marquez & Coimbra 2011). Chapter 15 describes various forecasting model inputs that have the potential to improve solar-forecasting accuracy.

Onsite measurements provide beneficial information to improve the accuracy of solar forecasting. Sfetsos & Coonick (2000) developed hour-ahead solar univariate and multivariate forecasting models based on ARIMA and ANNs. For the multivariate models, additional meteorological variables such as temperature, pressure, wind speed, and wind direction were considered as inputs to the forecasting process. Notwithstanding, the authors found only temperature and wind speed to be beneficial indicator variables according to an input selection scheme based on autocorrelations and cross-correlations. In Mellit et al., (2010), relative humidity, sunshine duration, air temperature, and solar irradiance (diffuse, GHI, and DNI) were used for hour-ahead forecasting of the hourly solar-irradiance time series using ANNs and the adaptive (so called α-prediction) model. Both of these models were applied to the diffuse, GHI, and DNI components. Reikard (2009) incorporated ground-based meteorological inputs into solar forecasts using various stochastic-modeling approaches at forecasting horizons of 5, 15, 30, and 60 min. In Marquez et al., (2013), a new methodology was presented for processing ground-based measurements to derive sky-cover indices. These indices were derived from a total-sky imager, and radiometric measurements from GHI and a thermal IR sensor, along with their historical time series, were used as predictor variables to forecast GHI at the hour-ahead time horizon.

A cloud-cover time series from an NWP was considered as input to stochastic-learning models in Perez et al., (2007) and Marquez & Coimbra (2011). Cao & Lin (2008) treated categorical cloud-cover information (overcast, sunny, cloudy, cloudy to sunny, etc.) as belonging to fuzzy sets that were defuzzied as part of a preprocessing stage in the forecast algorithm. Cloud classification was also applied by Chen et al., (2011), in which a self-organized map (SOM) was trained to classify the local weather type based on inputs from an online meteorological service; subsequently an ANN was trained to produce a 24-hour-ahead forecast.

One of the strengths of an ANN-based forecast is that it gives the model developer the ability to select several inputs for improving forecast accuracy. However, including extraneous input variables usually leads to unstable forecasts because a high dimensionality of the input dataset is more susceptible to

severe extrapolations and may require excessive training data and computational time. To avoid poor generalization, it is necessary to discriminate between useful, redundant, and extraneous information. Therefore, in terms of stochastic forecasting approaches, the preprocessing of input selection is one of the most critical stages, requiring significant attention and time resources (Cao & Lin 2008).

Forecast model inputs are often selected after observing the autocorrelations and cross-correlations between candidate inputs (Sfetsos & Coonick 2000). A weak point in applying autocorrelations and cross-correlations is that these techniques are derived from linearity assumptions. In other applications, the inputs are selected using iterative procedures (such as GAs) based on nonlinear methods that resort to testing the inputs directly and discarding those that have a neglible effect on the optimality of the input set (Crispim et al., 2008, Mellit 2008, Marquez & Coimbra 2011). The optimization of the input-selection method can be driven by the accuracy of the resulting forecasts (Crispim et al., 2008, Mellit & Pavan 2010); however, Marquez & Coimbra (2011) also presented an approach that is model independent and based on the gamma test (GT). They used ANNs in combination with an input selection procedure involving GT evaluations and genetic algorithms (GAs) (Jones 2004) and showed that additional NDFD-based meterological variables such as maximum temperature and probability of precipitation can be useful for improved same-day forecast accuracy.

8.2.5. Section Summary

PB models contribute to our overall understanding of the dynamic processes involved in solar forecasting, but they contain intrinsic limitations in data collection, error propagation, and the complexity of models that can be realistically implemented. However, these models alone are unlikely to cover a statistically representative portion of the solution space; that is, they are not "dispersive" enough. For example, several different NWP variations are often equally wrong in the timing of a ramp forecast. This is one side of the modeling spectrum, where the model is deterministic and reasonably complex, but limited in its ability to cover all the nonlinear and chaotic relationships that characterize atmospheric phenomena. At the other end of the spectrum lie the purely stochastic methods, in which there is no physical model per se (only nonlinear interactions between variables). However, the mathematical approach is flexible enough to cover a statistically significant portion of the solution space in an autocorrective process that can represent the complexity of the physical processes but may not necessarily yield an explicit model for all of the relationships involved (complex algebraic expressions are typically all that is available). Because stochastic-learning methods need to learn from the process, good-quality historical data are required for comparatively long periods, as compared to less need for historical data for most explicit,

deteministic PB models. Between these two extremes, there is room for hybrid models that take advantage of the strengths of both by minimizing the effects of their shortcomings, which include fundamental constraints in forecasting horizons, as discussed.

8.3. METRICS FOR EVALUATION OF SOLAR-FORECASTING MODELS

Before developing a metric for the evaluation of solar-forecasting methods, it is important to parameterize the quantities under study. A common example for normalizing solar-irradiance time series is the clear-sky index, which is used to detrend solar-irradiance time series from its deterministic component, such that

$$k_y(t) = \frac{y(t)}{y_{cs}(t)} \tag{8.1}$$

which equals the ratio of actual to clear-sky GHI (hereinafter I) if the variable under study is GHI:

$$kt = \frac{I(t)}{I_{CS}(t)} \tag{8.2}$$

8.3.1. Solar Resource Variability

The variability of solar irradiance at ground level is due to several factors such as the presence of participating gases in the atmosphere (H_2O, O_3, etc.), aerosols, cloud cover, and solar position (Badescu 2008); it is also strongly dependent on the local microclimate and the averaging timescale used. Most solar variability, however, can be attributed to cloud cover and solar position. The variability due to solar position is completely deterministic whereas the variability due to clouds is considered mostly stochastic because precise models for cloud dynamics have proven elusive. Since the portion of solar variability that is of most concern to forecast models is the cloud-induced (or stochastic) component (Rodriguez 2010; Hoff & Perez, 2010; Mills & Wiser, 2010), we refer to solar variability as the standard deviation of the step-changes of the ratio of the measured solar irradiance to that of a clear-sky solar irradiance, so that the diurnal variability is neglected:

$$V = \sqrt{\frac{1}{N}\sum_{t=1}^{N}\left(\frac{I(t)}{I_{\text{clear}}(t)} - \frac{I(t-1)}{I_{\text{clear}}(t-1)}\right)^2} = \sqrt{\frac{1}{N}\sum_{t=1}^{N}(\Delta kt)^2} \tag{8.3}$$

This formulation of variability is essentially the same as in Hoff & Perez (2010) and Lave & Kleissl (2010) except for the modification to include deterministic changes Δkt as in Mills & Wiser (2010). For small time intervals of less than 5

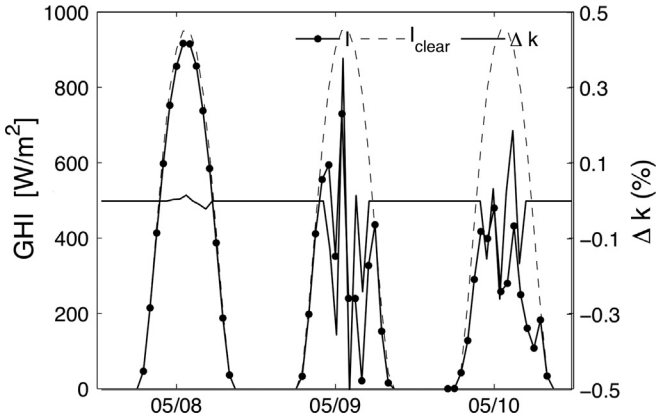

FIGURE 8.2 Time series of GHI (I) values, estimated clear-sky (I_{clear}), and calculated values of stochastic step-changes, Δk (hourly data for May 8–10, 2010, Merced, California).

min, this modification is not too important because the deterministic (solar position-dependent) variations are small. Figure 8.2 shows a plot of Δkt for a sequence of clear and cloudy days. For clear days, the fluctuations in Δkt are much smaller than for cloudy days, when large ramps are apparent in the Δkt time-series signal.

8.3.2. Conventional Metrics for Model Evaluation

Various metrics have been proposed and used to quantify the accuracy of solar forecasts. Determining which are most appropriate depends in part on the user: system operators need metrics that accurately reflect the costs of forecast errors, while researchers require indicators of the relative performance of different forecast models and that of a single model under different conditions. In addition to selecting a metric, an appropriate test dataset and analysis procedure are critical. First, the test dataset should exclude all data that were used to train models and develop postprocessing methods, so that evaluation is performed on independent data ("out-of-sample tests"). Also, data should be screened with appropriate quality-check procedures to ensure that forecast evaluation reflects forecast accuracy rather than issues with the observations used to test the forecasts (Beyer et al., 2009, Pelland et al., 2013).

Conventional performance metrics can be categorized according to three types of forecasting error: (1) bias, (2) variance, and (3) correlation. Hoff et al., (2012) summarize several absolute and relative statistical metrics for errors in forecasting and show that, at best, a large number of metrics are needed to provide a clear picture of the forecasting skill of any method. Here we summarize some of the most relevant conventional metrics before we propose an alternative solution to the problem of comparing different forecast accuracies across different microclimates, seasons, and time horizons in Section 8.3.

Bias characterizes the balance between over- and underprediction. The most used bias measure is mean bias error (MBE), defined as

$$MBE = \frac{1}{N}\sum_{t=1}^{N}\left(I(t) - \hat{I}(t)\right) \tag{8.4}$$

where $I(t)$ is the irradiance measured at time t, $\hat{I}(t)$ is the forecasted irradiance value at time t, and N is the number of data points in the set. This metric returns a 0 value for situations of perfect forecasts ($\hat{I}(t) = I(t)$) and for situations where the positive and negative errors simply cancel out by summing to 0. Because forecast methods are usually site specific, MBE is normally not a major concern when comparing multiple forecasting models for the same sensor output, because it can be effectively fixed in postprocessing through bias corrections. In contrast, in solar radiation modeling, whose purpose is to predict solar irradiation where sensors are not available, it is important to carefully consider the magnitude of MBE, as solar-radiation models are used for long-term solar-resource assessments.

The coefficient of determination R^2 measures how well forecast values predict trends in measured values. It is a comparison of the variance of the errors to the variance of the data to be modeled:

$$R^2 = 1 - \frac{\sigma^2\left(\hat{I} - I\right)}{\sigma^2(I)} \tag{8.5}$$

where σ^2 is the variance of the dataset and not to be mistaken for the variability defined in equation 8.3 ($\approx \sqrt{\sigma^2(\Delta k)}$). For perfect forecasting, R^2=1. The value of R^2 can be directly related to the RMSE (equation 8.6) by noticing that

$$R^2 \sim 1 - \frac{RMSE^2}{var(I)} \tag{8.6}$$

There are two commonly used metrics to evaluate the variance of forecast errors: the root mean square error (RMSE) and the mean absolute error (MAE). The RMSE value is related to the standard deviation of the errors. Both MAE and RMSE indicate the amount of spread in the errors and in some sense represent the 1- and 2-norms of the errors. Note that over- and underpredictions are not differentiated by the RMSE and MAPE. However, a bias automatically increases MAE and RMSE. To isolate the random component of RMSE, the standard relative error is often used. The RMSE is calculated as

$$RMSE = \sqrt{\frac{1}{N}\sum_{t=1}^{N}\left(\hat{I}(t) - I(t)\right)^2} \tag{8.7}$$

where the summation is carried over the entire dataset. Night values are typically removed in the above calculations of R^2 and RMSE, and a single value is given to summarize the overall quality of the forecast for the entire dataset.

Normalization can occur relative to energy produced or capacity; utilities tend to prefer the latter (which is more favorable by a factor ~4), while scientists tend to prefer the former. Again, none of these metrics embed a sense of variability in the irradiance time-series data. For example, both Perez et al., (2010) and Müller & Remund (2010) found that the RMSE forecast error is lower in places with sunnier (less variable) weather conditions. Similarly, Lorenz et al., (2009), Mathiesen & Kleissl (2011), and Pelland et al., (2011) found that RMSE decreases when NWP output is spatiallly averaged (i.e., when variability is reduced).

Other metrics quantify the ability of a model to reproduce observed frequency distributions (see Chapter 10). The Kolmogorov-Smirnoff integral (*KSI*) metric (equation 8.9) is obtained by integrating the absolute difference between the modeled $\varphi(\hat{I})$ and the measured $\varphi(I)$ cumulative frequency distributions. The result is normalized by the Kolmogorov-Smirnov critical value V_c, which depends on the number of available data samples (the higher the number of experimental data samples, the closer the modeled distribution to the actual distribution).

$$KSI = \frac{\int_0^{I_{\max}^{ref}} \left|\varphi\left(\hat{I}\right) - \varphi(I)\right| dI}{V_c} \tag{8.8}$$

A *KSI* score on the order of or better than 100% is generally considered acceptable. An interpretation of this is that the mean absolute difference between the measured and modeled distributions is equal to or smaller than the critical difference.

The OVER metric (see equation 10.5 in Chapter 10) is based on *KSI* but integrates only differences between the cumulative frequency distributions that are larger than a threshold determined by the number of considered data points. An OVER score of 0% indicates that the model always differs from the measurement by less than the threshold.

A practical option is to use MAE and MAPE as standard evaluation metrics since they are are less sensitive to large errors and inclusion or exclusion of nighttime data.

8.3.3. A Time Horizon–Invariant (THI) Metric

Here we define uncertainty as the standard deviation of a model forecast error divided by the estimated clear-sky value of the solar irradiance over a subset time window of N_w data points:

$$U = \sqrt{\frac{1}{N_w}\sum_{t=1}^{N_w}\left(\frac{\hat{I}(t) - I(t)}{I_{\text{clear}}(t)}\right)^2} \tag{8.9}$$

This definition is related to the commonly used RMSE normalized with respect to average irradiance. Our definition is similar except that the normalization is made with respect to I_{clear} for which we use a third-order polynomial fit $I_{\text{clear, poly}}$ in our evaluations (for a study of the effect of different clear-sky model approximations, refer to Marquez & Coimbra 2013).

The following metric directly evaluates the variability effectively reduced by the forecasting models by taking the difference between U and V and normalizing it with respect to V:

$$S = \frac{V - U}{V} \tag{8.10}$$

where U and V are calculated over the same dataset. The metric for evaluating the quality of forecast models is more simply computed by considering the ratio between uncertainty, U, and variability, V, such that

$$S = 1 - \frac{U}{V} \tag{8.11}$$

The forecast skill defined above is such that when $s = 1$ the solar forecast is perfect, and when $s = 0$ the forecast uncertainty is as large as the variability. By definition, the persistence model should have a forecast skill $s = 0$. Consequently, the ratio $\frac{U}{V}$ is a measure of improvement over the persistence forecast when the latter is corrected by the clear-sky index (or, in other words, when diurnal variability of the clear sky is taken into consideration). A negative value for s implies that the model performs worse than the corrected persistence forecast. Forecast models that improve on persistence are characterized by s values between 0 and 1, with higher values indicating better forecast skill. Also note that when V is small, U is also small (easy to forecast) and when V is large, U is typically large as well. Definition (8.11) is consistent with the general perception of forecasting skill, particularly when all deterministic components are removed.

Since U and V are random variables, it follows that s is also a random variable. To obtain a representative value of s, we take the average value $[s]$ as the indication of forecast skill. The average is obtained by calculating U and V for various time-window subsets. The time windows are selected by fixing N_w (the window size) and computing U_j and V_j over each jth window in the time series ($N_w = 500$ in Figure 8.3). Night values are not included in Figure 8.3, nor are they used in the calculations below. If a time window contains a large number of clear days, both U (forecasting error) and V (solar-irradiance variability) are expected to be small for that time window; thus, the relative amount of error relative to variability is preserved. Likewise, if the forecast-averaging time step is small (1 min vs. 1 h forecasts) or if a spatially averaged forecast variable is considered (such as in fleet-power forecasts), both U and V are expected to be smaller and their ratio defines an invariant or at least less variant metric.

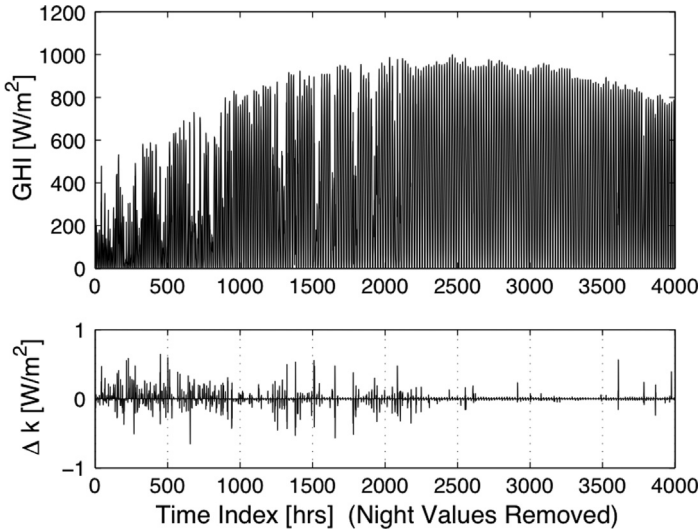

FIGURE 8.3 Time series (in hours) of solar irradiance I and Δk for January 1 to October 31, 2011, Merced, California. The time series is partitioned into window sizes of N_w=500 h. Each vertical line in the lower graph represents the boundaries of the 500 h time windows (note that night values have been removed). Lower-quality experimental values due to electrical power issues in May and July were removed.

8.4. APPLYING THE THI METRIC TO EVALUATE PERSISTENCE, AND NONLINEAR AUTOREGRESSIVE FORECAST MODELS

8.4.1. NAR and NARX Forecasting Models

For illustration purposes, the THI metric proposed is now applied to two stochastic solar-forecasting models based on ANNs. We employ feedforward ANNs to approximate future hourly values of $I(t)$ using lagged values of the time series. The forecasting performances are evaluated based on conventional metrics (Section 8.3.2) and the proposed metric (s) in order to compare and contrast the quality of the models.

The first forecast model includes only the hourly-average $I(t)$ time series as input and is referred to as the nonlinear autoregressive (NAR) forecasting model. A second model including additional inputs is referred to as the nonlinear autoregressive with exogenous inputs (NARX) forecasting model. The NAR model for 1-hour-ahead predictions can be mathematically expressed as

$$I(t+1) = f(I(t), I(t-1), \ldots, I(t-n)) \tag{8.12}$$

where $n + 1$ is the number of time delays of the time series $I(t)$ that are used as inputs to predict $I(t + 1)$. Here we set the number of time delays to 2 (i.e., only $I(t)$ and $I(t - 1)$ are used to predict $I(t + 1)$). The function f is

based on a feedforward ANN structure where the number of hidden neurons is set to 10 for this example. The network weight values are determined by the "early-stopping" method for ANN training where the data are split into three sets: a training set for computing directional derivatives of the errors in weight space, a testing set for determining when to stop training, and a validation set, which is not used at all during the ANN training (Bishop 1995). Data from October 15–31, 2010, are used for validation; the remaining data, from January 1, 2010, through October 14, 2010, are split randomly into 80% for the training set and 20% for the testing sets. The ANNs are implemented using the MATLAB Neural Network Toolbox Version 7.0.

The NARX model is similar to the NAR model except that more time-series signals are utilized in the forecast scheme:

$$I(t+1) = f(I(t), I(t-1), \ldots, I(t-n), u_1(t), u_2(t-1), \ldots u_m(t-n)) \quad (8.13)$$

where m is the number of exogenous inputs. In this case, u represents 30 min and 6 min backward moving averages (MA) and standard deviations (SD) of clearness-index values, which are calculated from 30 s-interval data, denoted k' to distinguish them from k. The symbol k is reserved for the clear-sky index for hourly averages of I. These inputs are an attempt to use the trends at the last moments of the current hour to forecast the next 1 h time step. The NARX model contains more input neurons than does the NAR model and the number of time delays is set to 2 for each signal. The number of hidden neurons is also set to 10, and the early-stopping method is used for adjusting the weights.

8.4.2. Comparison of Forecasting Models and Persistence

The forecast-quality evaluations were performed for the dataset collected from January 1 through October 31, 2010 (Marquez & Coimbra 2013). Figure 8.4 shows scatter plots of U_j versus V_j computed for each jth time-window partitioning of the dataset for N_w = 50, 100, 150, and 200 h. These plots allow us to visualize

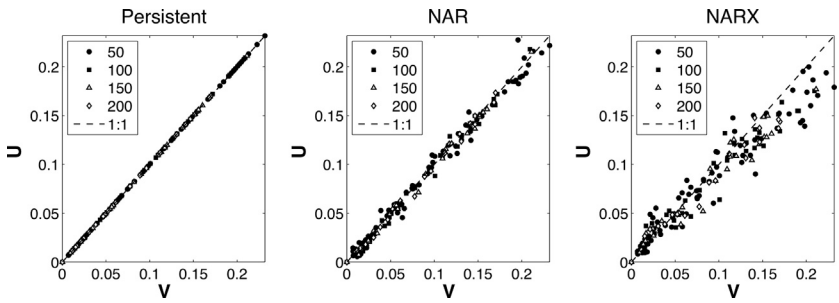

FIGURE 8.4 Scatter plot of U and V for the persistence, NAR, and NARX models using a polynomial fit as a clear-sky model for normalization. *Light-gray dashed lines* mark the identity (1:1) line. (From Marquez & Coimbra, 2013.)

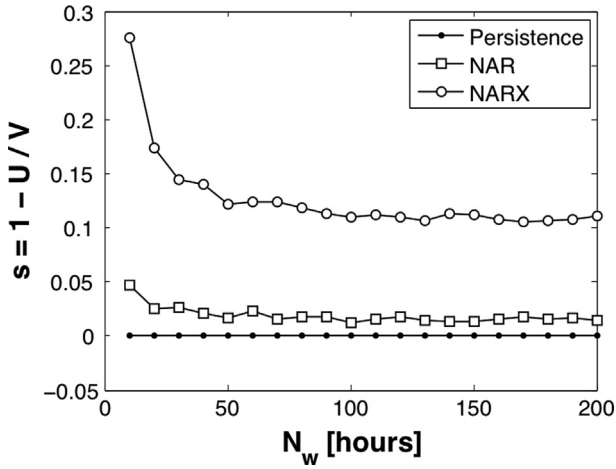

FIGURE 8.5 THI forecast-quality metrics for the persistence, NAR, and NARX models on validation and training datasets as a function of time-window size in hours. For comparison, the metric $s = 1 - \frac{U}{V}$ is based on a polynomial fit for clear-sky conditions. NARX is the *top curve* in all plots, whereas persistence is the *flat line* for $s = 0$.

the forecasting performance over various time-window subsets with different variability values. They show that the persistence models result, as expected, in $s = 0$, since $U_j = V_j$ for all windows. The NAR model forecast quality is only as good as persistence, while the NARX model does show some significant forecasting skill, which is clear from the many scatter points that fall below the 1:1 line.

The forecast skill s is a random variable that depends explicitly on the ratio $\frac{U}{V}$. The statistical average of this ratio is approximated by computing the slope of the scatter points as shown in Figure 8.4, since the scatter plots from each of the models form an almost linear relationship.[1] The slopes are evaluated using $N_w = 10, 11, \ldots 200$ (see Figure 8.5). Values of the average $[s]$ converge to a certain value as N_w increases. For the persistence model $[s]=0$, for the NAR model $2\% < [s] < 5\%$, and for the NARX model $10\% < [s] < 15\%$. These results are invariant with the use of different clear-sky models for normalization (see Marquez & Coimbra 2013 for a more detailed discussion).

Numerical values of $[s]$ obtained using $N_w=200$ are given in Table 8.3, along with the more common forecast quality metrics, R^2 and RMSE. The value of R^2, which ranges from 0.964 to 0.977 for the validation dataset, gives the impression that even the persistence forecast for $N_w=200$ is very accurate, which highlights the fact that this performance measure (R^2) is inadequate because, by definition, the persistence model fails to capture any future

1. Throughout this chapter, we use a linear relationship between U and V to illustrate the metric. It is relatively straightforward to consider nonlinear and piecewise relations between U and V.

TABLE 8.3 Evaluation of Error Metric $\langle s \rangle = 1 - \frac{U}{V}$ for Different Forecast Models.

Model	R^2	RMSE (W/m^2)	$s = 1 - \frac{U}{V}$ (%)
Persistence	0.934	56.5	0.00
NAR	0.924	60.2	−2.56%
NARX	0.949	49.4	16.12%

Note: All values correspond to the validation set only.

information on solar-irradiance variability. Similarly, the RMSEs, which range from 48.8 to 59.4 W/m^{-2}, appear low if compared to other RMSEs in the literature without considering the solar-irradiance variability conditions in those studies. The point here is that both the R^2 and RMSE metrics do not directly translate into forecast skill. On the other hand, the $[s]$ metric reveals that the persistence model has 0 forecasting skill since $[s] = 0$, which implies that $U = V$ (all the uncertainty is due to the variability). Below we show that normalizing the RMSE values in the table by the persistence RMSE provides a metric similar to $[s]$.

The NAR and NARX models are compared by observing the improvements over persistence, which are approximate to the proposed metrics $-\frac{U}{V} \sim \frac{RMSE}{RMSE_p}-$where RMSE$_p$ is the RMSE of the persistence model. To show this relation, the RMSEs of the persistent, NAR, and NARX models were calculated again using the value of N_W=200 h; then the RMSEs of the NAR and NARX forecasts versus the RMSEs of the persistence model were plotted, as shown in Figure 8.6. The slopes obtained by the regression fits are equivalent

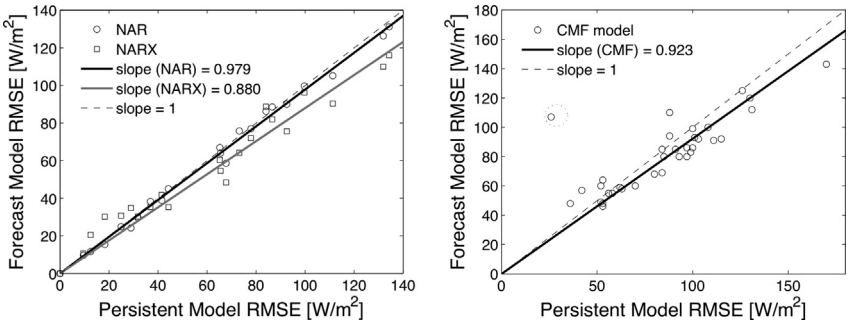

FIGURE 8.6 RMSE of different forecast models vs. RMSE of the persistence model. (a) NAR and NARX models; (b) CMF model. The point highlighted with a *dashed circle* was ignored for calculating the regression line for the CMF model. (From Marquez & Coimbra 2013.)

to the slopes for the average of the ratio $\frac{U}{V}$. Taking the slope values to estimate $[s]$, we obtain values of $[s] = 1 - 0.979 = 2.1\%$ and $[s] = 1 - 0.880 = 12.0\%$, which approximate closely the values in Table 8.3 for the NAR and NARX models, respectively. The close relation between $\frac{U}{V}$ and $\frac{RMSE}{RMSE_p}$ can also be established from the definitions of U, V, and $RMSE$ and by realizing that the normalization factors effectively cancel out when taking these ratios. Estimating $\frac{U}{V}$ by calculating $\frac{RMSE}{RMSE_p}$ is much easier than the procedure used to generate the graphs in Figure 8.4, so this approach is recommended. However, we emphasize here the rationale for proposing the metric, which is that it gives a measure of the effective reduction of random variability (equation 8.11).

8.4.3. Comparison with a Satellite Cloud-Motion Forecast Model

In this section, we show how the NAR and NARX models compare to the forecast model by Perez, et al., (2010), which is also described in Chapter 10. The Perez model is based on cloud-motion forecasts (CMF) and was used to validate solar-irradiance forecasts 1–5 h ahead for several climatically distinct sites for August 23, 2008, through August 31, 2009. In the CMF technique, satellite-derived images are used to extract pixel values of the clear-sky index kt at time t. The motions of the clouds are then predicted and used to determine future images from which values of $k(t + 1)$ are inferred. From the $k(t + 1)$ predictions, solar-irradiance forecasts are obtained. The CMF approach is relevant for comparisons to our clear-sky and NAR/NARX models because persistence models in both studies make use of the current clearness index value to predict future values of solar irradiance.

In Table 10.2 in Chapter 10, RMSEs for 1-hour-ahead forecasts of the CMF model and the persistence model are given. These values were used to produce Figure 8.6, where we calculate a regression line after setting the intercept value at 0. Just like the value of $[s]$ for the NAR and NARX models from Figure 8.4, the $[s]$ value of the CMF model is estimated to be $1 - 0.923 \sim 8\%$. This value is close to the value obtained by the NARX model value reported here; therefore, a NARX-type approach seems to produce forecasting performance comparable to that of the CMF-model approach for the 1-hour-ahead time horizon.

8.5. CONCLUSIONS

Methods of solar forecasting range from physical to stochastic depending on available data inputs and resources and, to a large degree, on the forecasting time horizons of interest. As discussed, both physical and stochastic approaches

have significant strengths and weaknesses. One possible way to overcome the weaknesses of individual methods is to develop hybrid methodologies that capitalize on the strengths of both approaches so that the end result is a forecasting system that is robust, flexible, and accurate.

Because solar-forecasting applications are developed and evaluated at different time periods and locations, and because of a lack of consensus on error metrics, judging the relative strengths or weaknesses of a given approach is generally difficult. As interest grows in the impacts of high solar penetration, more robust metrics will be needed. The evaluation algorithm described in this chapter provides a measure based on the variability of the solar resource and has the potential to become one of the benchmark metrics for solar-forecasting evaluations.

REFERENCES

Bacher, P., Madsen, H., Nielsen, H.A., 2009. Online short-term solar power forecasting. Solar Energy 83, 1772–1783.

Badescu, V., 2008. Modeling Solar Radiation at the Earth Surface. Springer-Verlag, Berlin Heidelberg.

Bishop, C.M., 1995. Neural networks for pattern recognition. Oxford University Press, Oxford.

Breitkreuz, H., Schroedter-Homscheidt, M., Holzer-Popp, T., Dech, S., 2009. Short-range direct and diffuse irradiance forecasts for solar energy applications based on aerosol chemical transport and numerical weather modeling. Journal of Applied Meteorology and Climatology 48, 1766–1779.

Cao, J., Lin, X., 2008. Application of the diagonal recurrent wavelet neural network to solar irradiation forecast assisted with fuzzy technique. Engineering Application of Artificial Intelligence 21, 1255–1263.

Chen, C., Duan, S., Cai, T., Liu, B., 2011. Online 24-h solar power forecasting based on weather type classification using artificial neural networks. Solar Energy 85 (11), 2856–2870.

Chow, C.W., Urquhart, B., Lave, M., Dominquez, A., Kleissl, J., Shields, J., et al., 2011. Intrahour forecasting with a total sky imager at the UC San Diego solar energy testbed. Solar Energy 85, 2881–2893.

Crispim, E.M., Ferreira, P.M., Ruano, A.E., 2008. Prediction of the solar radiation evolution using computational intelligence techniques and cloudiness indices. International Journal of Innovative Computing Information and Control 4 (5), 1121–1133.

Hammer, A., Heinemann, D., Lorenz, E., Ckehe, B.L., 1999. Short-term forecasting of solar radiation: a statistical approach using satellite data. Solar Energy 67, 139–150.

Hammer, A., Heinemann, C., Hoyer, C., Lorenz, E., 2001. Satellite based short-term forecasting of solar irradiance–comparison of methods and error analysis. The 2001 EUMETSAT Meteorological Satellite Data User's Conference, 677–684.

Hammer, A., Heinemann, D., Hoyer, C., Kuhlemann, R., Lorenz, E., Miller, R., et al., 2003. Solar energy assessment using remote sensing technologies. Remote Sensing of Environment 86, 423–432.

Hoff, T.E., Perez, R., 2010. Quantifying PV power output variability. Solar Energy 84 (10), 1782–1793.

Hoff, T.E., Perez, R., Kleissl, J., Renne, D., Stein, J.S., 2012. Reporting of irradiance model relative errors, Proceedings of the 2012 ASES Annual Conference. Rayleigh, NC.

Jones, A.J., 2004. New tools in non-linear modelling and prediction. Computational Management Science 1 (2), 109–149.

Lave, M., Kleissl, J., 2010. Solar variability of four sites across the state of Colorado. Renewable Energy 35 (12), 2867–2873.

Lorenz, E., Hurka, J., Heinemann, D., Beyer, H.G., 2009. Irradiance forecasting for the power prediction of grid-connected photovoltaic systems. IEEE Journal of Selected Topics in Applied Earth Observations and Remote Sensing 2 (1), 2–10.

Marquez, R., Coimbra, C.F.M., 2011. Forecasting of global and direct solar irradiance using stochastic learning methods, ground experiments and the NWS database. Solar Energy 85 (5), 746–756.

Marquez, R., Coimbra, C.F.M., 2013. Intrahour DNI forecasting methodology based on cloud tracking image analysis. Solar Energy (91), 327–336.

Marquez, R., Coimbra, C.F.M., 2013. A proposed metric for evaluation of solar forecasting models. ASME Journal of Solar Energy Engineering (135). Art. #0110161.

Marquez, R., Pedro, H.T.C., Coimbra, C.F.M., 2013. Hybrid solar forecasting method uses satellite imaging and ground telemetry as inputs to ANNs. Solar Energy (92), 172–188.

Marquez, R., Gueorguiev, V.G., Coimbra, C.F.M., 2013. Forecasting solar irradiance using sky cover indices. ASME Journal of Solar Energy Engineering (135). Art. #0110171.

Mathiesen, P., Kleissl, J., 2011. Evaluation of numerical weather prediction for intra-day solar forecasting in the continental United States. Solar Energy 85 (5), 967–977.

Mellit, A., Pavan, A.M., 2010. A 24-h forecast of solar irradiance using artificial neural network: application for performance prediction of a grid-connected PV plant at Trieste, Italy. Solar Energy 84 (5), 807–821.

Mellit, A., Eleuch, H., Benghanem, M., Elaoun, C., Pavan, A.M., 2010. An adaptive model for predicting of global, direct and diffuse hourly solar irradiance. Energy Conversion and Management 51 (4), 771–782.

Mellit, A., 2008. Artificial intelligence technique for modelling and forecasting of solar radiation data: a review. International Journal of Artificial Intelligence and Soft Computing 1, 52–76.

Mills, A., Wiser, R., 2010. Implications of wide-area geographic diversity for short-term variability of solar power. Technical report, Lawrence Berkeley National Laboratory Technical Report LBNL-3884E.

Paoli a, C., 2010. Forecasting of preprocessed daily solar radiation time series using neural networks. Solar Energy 84 (12), 2146–2160.

Pedro, H.T.C., Coimbra, C.F.M., 2012. Assessment of forecasting techniques for solar power output with no exogenous inputs. Solar Energy (86), 2017–2028.

Pelland, S., Galanis, G., Kallos, G., 2011. Solar and photovoltaic forecasting through post-processing of the Global Environmental Multiscale numerical weather prediction model. Prog. Photovolt. Res. Appl. http://dx.doi.org/10.1002/pip.1180.

Pelland, S., Remund, J., Kleissl, J., Oozeki, T., de Branbadere, K., 2013. Photovoltaic and Solar Forecasting: State of the Art, International Energy Agency (IEA) Photovoltaic Power Systems Programme, Task 14. Subtask 3.1 Report IEA-PVPS, T14–01.

Perez, R., Moore, K., Wilcox, S., Renne, D., Zelenka, A., 2007. Forecasting solar radiation - Preliminary evaluation of an approach based upon the national forecast database. Solar Energy 81, 809–812.

Perez, R., Kivalov, S., Schlemmer, J., Hemker, K., Renne, D., Hoff, T.E., 2010. Validation of short and medium term operational solar radiation forecasts in the US. Solar Energy 84 (5), 2161–2172.

Reikard, G., 2009. Predicting solar radiation at high resolutions: A comparison of time series forecasts. Solar Energy 83 (3), 342–349.

Rodriguez, G.D., 2010. A utility perspective of the role of energy storage in the smart grid. April 2010 IEEE Power and Energy Society General Meeting. New Orleans.

Schroedter-Homscheidt, M., Hoyer-Klick, C., Rikos, E., Tselepsis, S., Pulvermüller, B., September 2009. Nowcasting and forecasting of solar irradiance for energy electricity generation, SolarPACES. Berlin, Germany.

Sfetsos, A., Coonick, A.H., 2000. Univariate and multivariate forecasting of hourly solar radiation with artificial intelligence techniques. Solar Energy 68 (2), 169–178.

Velden, C.S., Olander, T.L., Wanzong, S., 1998. The impact of multispectral GOES-8 wind information on Atlantic tropical cyclone track forecasts in 1995. Part i: dataset methodology, description, and case analysis. Monthly Weather Review 126, 1202–1218.